ACS OMEGA

http://pubs.acs.org/journal/acsodf

Article

Conformationally Restricted Dipeptide-Based Nanoparticles for Delivery of siRNA in Experimental Liver Cirrhosis

Saikat Biswas, Nitin Yadav, Pinky Juneja, Akash Kumar Mourya, Savneet Kaur, Dinesh M. Tripathi,* and Virander Singh Chauhan*

Cite This: *ACS Omega* 2022, 7, 36811−36824

Read Online

ACCESS | Metrics & More | Article Recommendations | Supporting Information

ABSTRACT: Liver cirrhosis is a major health problem with multiple associated complications. The presently available drug delivery systems showed moderate site-specific delivery of antifibrotic molecules to the diseased liver; therefore, research on more effective and selective delivery systems in the context of liver cirrhosis remains a necessity in clinical investigation. The aim of the present study was to develop a peptide-based targeted nanocarrier to deliver an oligonucleotide to the hepatic sinusoidal and perivascular regions of the cirrhotic liver. We have synthesized and characterized a conformationally restricted targeted pentapeptide (RΔFRGD), which contains an unnatural amino acid, α,β-dehydrophenylalanine (ΔF). The RΔFRGD self-assembled into spherical nanoparticles (NPs) and was characterized by dynamic light scattering (DLS) and transmission electron microscopy (TEM). Next, we investigated the delivery potential of the pentapeptide-based NPs to make a stable complex with a well-established small interference RNA and studied its site-specific delivery in experimental liver cirrhosis. We used siNR4A1 of the orphan nuclear receptor 4A1 (NR4A1), a well-known regulatory checkpoint for controlling liver fibrosis. Peptide NPs and their complex with siNR4A1 showed high biocompatibility against various mammalian cell lines. Hepatic tissue biodistribution analysis illustrated that targeted NPs predominantly accumulated in the cirrhotic liver compared to normal rats, specifically in sinusoidal and perivascular areas. A significant downregulation of the NR4A1 mRNA expression (−70%) andlower levels of the NR4A1/GAPDH ratio (−55%) were observed in the RΔFRGD-siNR4A1 nanocomplex-treated group in comparison to the RΔFRGD-vehicle group (RΔFRGD-Veh) at the gene and protein levels, respectively. In addition, *in vivo* inhibition of NR4A1 produced a significant aggravation in hepatic fibrosis compared with siRNA-vehicle-treated rats (+41% in the MT stain). The novel pentapeptide-based targeted delivery system can be further evaluated and validated for therapeutic purposes in various pathological conditions.

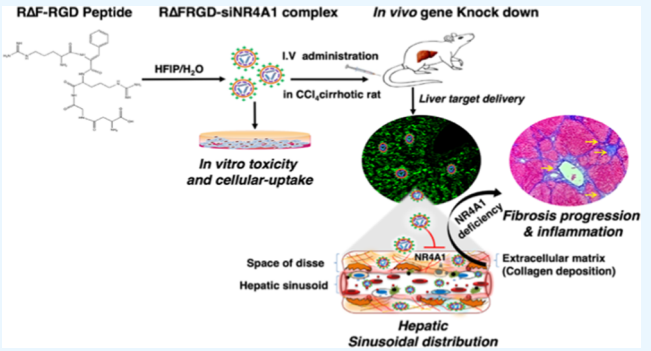

1. INTRODUCTION

Chronic liver disease and cirrhosis are major socioeconomic burdens worldwide that have been steadily increasing over the last few decades. According to a recent Global Burden of Disease's (GBD) study, morbidity and mortality caused by liver fibrosis exceeded 1.32 million worldwide.[1] Liver cirrhosis caused by drugs, viral infections, alcohol, or lipid toxicity is associated with excessive tissue remodeling and abnormal deposition of excess extracellular matrix (ECM) proteins.[2,3] Activated hepatic stellate cells (aHSCs) are the major cells that secrete an excessive amount of collagen in the Disse Space leading to hepatic fibrosis.[4−6] This advanced pathological progression is irreversible and eventually leads to serious clinical symptoms such as ascites, portal hypertension, hepatic encephalopathy, etc.[7] Although several antifibrotic molecules are under various stages of clinical development, successful hepatic pharmacotherapy has remained an unmet challenge for liver cirrhosis due to poor therapeutic efficiency, rapid hepatic clearance, and limited targeted delivery systems with desirable safety profiles.[8,9] To accelerate the preclinical development of antifibrotic agents or gene therapy, efficient and specific targeted delivery systems must accompany *in vivo* validation.[10]

Over the last few decades, the introduction of oligonucleotides (siRNA, miRNA, shRNA) into cells has been done with the aim to prevent, halt, or reverse diseased conditions including cancer.[11] While small interference RNA (siRNA) is a promising tool for understanding the disease mechanism and/or developing therapy, a fundamental challenge of gene delivery is the development of a safe and efficient delivery

Received: August 17, 2022
Accepted: September 19, 2022
Published: October 4, 2022

https://doi.org/10.1021/acsomega.2c05292
ACS Omega 2022, 7, 36811−36824

system.[12] Effective siRNA delivery requires an appropriate carrier system that should assist with siRNA delivery, protect it from environmental conditions, and provide an enhanced cellular internalization with controlled release.[13] Targeted delivery using site-specific nanoparticles (NPs) may serve as an efficient platform for oligonucleotide delivery because of their ability to evade normal cells.[14] Although many efforts are being made for developing liver-targeting carrier systems, there have been few reports describing the development of nanocarrier-based specific targeting of the cirrhotic liver.[15] Examples include human serum albumin (HSA)-coupled mannose-6-phosphate (M6P), retinol-modified liposomes, cyclic peptide cyclo (S-R-A-N-L-I-D-C) and cyclo (C-G-R-G-S-P-K)-conjugated particles, etc.[16−18] However, most of these systems lack specificity because they target both quiescent and activated HSCs and some of them also affect scavenger receptors on the endothelial cells and Kupffer cells.[19]

The development of peptide-based nano delivery systems has become an area of active investigation. Self-assembly of naturally occurring or nonprotein amino acid-containing peptides into ordered nanostructures has been widely investigated, particularly as delivery platforms for small oligonucleotides.[20] Short peptide-based nanostructures (2−5 residues) have gained more attention owing to their simple structure, ease of synthesis, low cost, and, above all, high biocompatibility.[21,22] However, the susceptibility of peptide-based systems to enzymatic degradation remains a hurdle in their clinical development.[23] Ultrashort peptide-based nanostructures containing a chemically modified amino acid, α,β-dehydrophenylalanine (ΔF) residue, have been shown to self-assemble into various nanostructures with characteristic shapes and sizes.[24−27] The presence of ΔF in peptide sequences induces conformational restriction as well as resistance to enzymatic degradation.[24,27] Dipeptides containing ΔF have been successfully utilized for the delivery of drugs, antigens, and oligonucleotides in *in vitro* and *in vivo* conditions.[28−31]

In this study, we have designed a novel pentapeptide (RΔFRGD) using a highly stable self-assembling dipeptide template, containing arginine-α,β-dehydrophenylalanine (RΔF), and a tripeptide, arginine-glycine-aspartic acid (RGD), a well-known shortest fragment of fibronectin responsible for cellular adhesion processes. The homing ligand RGD has been reported to enhance the accumulation of nanocarriers at the liver cirrhotic site and assist in cytosolic and endosomal localization of NPs.[32,33] We have investigated the self-assembling properties of RΔFRGD into nanoparticles and fully characterized them. We explored whether the peptide NPs will condense and deliver a siRNA, specific and relevant to the fibrotic liver condition. To provide a proof of principle, we selected an siNR4A1 from the orphan nuclear receptor 4A1 (NR4A1, also known as NUR77). NR4A1 is an endogenous inhibitor of transforming growth factor signaling (TGF-β) and fibrogenesis.[34−36] Lack of active NR4A1 has been reported to cause pathological tissue fibrosis.[34] Successful delivery of siNR4A1 will be expected to silence the NR4A1 gene, resulting in a decrease in the expression level of NR4A1 and an increase in fibrosis. Here, we described the condensation of siNR4A1 with the pentapeptide-based NPs to carry siNR4A1 and its preferential delivery to the sinusoidal area of the cirrhotic liver. The pentapeptide readily condenses to form a stable and highly biocompatible complex. Our *in vitro* and *in vivo* studies have clearly shown that the pentapeptide NPs can efficiently bind and deliver siNR4A1 to the hepatic sinusoidal region of the fibrotic liver. The pentapeptide NPs may be further investigated for the delivery of functional oligonucleotides and biomolecules to the fibrotic liver.

2. MATERIALS

We bought the following compounds from Novabiochem: Fmoc-Arg(pmc)-OH, Fmoc-Gly-OH, and Fmoc-Asp(otBu)-OH. *N*-Methyl morpholine, sodium hydroxide, sodium chloride, tetrahydrofuran, isobutyl chloroformate, DL-3-phenylserine hydrate, sodium bicarbonate, trifluoroacetic acid, triisopropylsilane, dimethyl sulfoxide, and anhydrous sodium acetate were purchased from Sigma. We bought acetic anhydride from SD Fine Chem Limited, India. Methanol, sodium sulfate, acetonitrile, and diethyl ether were purchased from Merck, Germany. USA-based Gibco supplied DMEM, RPMI, and collagenase type 1. Fetal bovine serum, citric acid, MTT, sterile water, trypsin EDTA, PBS, 100-μm nylon strainer, and trypan blue were received from HIMEDIA, India. We bought ELISA kits from Invitrogen, Germany. CCl_4 (Merck, Bangalore, India), NR4A1 siRNA (Eurogentec, Belgium), NR4A1 antibody (Thermo Fisher Scientific), isoflurane (Baxter, Thane, India), ketamine (Neon, Delhi, India), midazolam (Neon, Delhi, India), and scalp vein set (Romsons Medsource, Delhi, India) were also used. Percoll was obtained from GE Healthcare, Chicago.

3. METHODS

3.1. Synthesis and Characterization of RΔFRGD and Fluorescent Labeling. Fmoc-Arg(Pmc)-ΔPhe azlactone was synthesized (5−10 mM) by the solution-phase synthesis procedure, and the details are given in Text S1.[23−26] RΔFRGD and the corresponding natural analogue were synthesized using standard Fmoc chemistry on the rink amide MBHA (4-methyl benzhydryl amine hydrochloride salt) resin in the manual mode with DIC and oxymaPure as coupling agents, and details are provided in Text S2.[37] RΔFRGD was characterized using a Shimadzu RP-HPLC with a Phenomenex C-18 column. A binary gradient of acetonitrile−water (5−95%, 0.1% TFA) mobile phase (1 mL/min) for 45 min was used. Electron spray ionization mass spectrometry (Applied Biosystems QStar (Q-TOF)) was used to determine the molecular mass of RΔFRGD (0.1 mg/mL dipeptide in LC-MS-grade acetonitrile and 0.1% formic acid). For labeling of RΔFRGD with fluorescein isothiocyanate isomer I (FITC), we followed a protocol given in Text S3.[30]

3.2. Self-Assembly of RΔFRGD into Nanoparticles. The self-assembly of RΔFRGD was investigated at different peptide concentrations (1−5 mg/mL). Peptide dissolved in HFIP (50 μL for 1 mg) and the self-assembly of RΔFRGD was initiated by adding peptide solutions to deionized water (950 μL) and kept aside for ∼2 h at room temperature. To remove HFIP from nanoparticles, preformed NPs were lyophilized and resuspended in Milli-Q water at 2 mg/mL.

3.3. Characterization of Pentapeptide NPs Using Dynamic Light Scattering (DLS). Hydrodynamic size measurements for RΔFRGD NPs were performed using a Malvern Zetasizer Nano Series Nano ZS90, and the specific experimental procedures have been previously described.[30,31,38]

3.4. Loading of siNR4A1 onto RΔFRGD NPs. siNR4A1 was provided by Eurogentec (Seraing, Belgium). The RΔFRGD-siNR4A1 nanocomplex was prepared with a fixed

https://doi.org/10.1021/acsomega.2c05292
ACS Omega 2022, 7, 36811−36824

amount of siNR4A1 (500 ng) at a different ratio of preformed RΔFRGD NPs including 1:20, 1:30, 1:40, 1:50, and 1:100 (siNR4A1/NPs, w/w) followed by a vortex for 30 s to initiate the complex formation. The samples were incubated for 1 h at room temperature with constant gentle stirring. Condensation of siNR4A1 with RΔFRGD NPs was confirmed by a conventional gel retardation assay. The samples were run on a 3% agarose gel (containing EtBr) in 1× TAE at 60 V for 60 min. The image was taken using a UV transilluminator (Bio-Rad Laboratories, Inc.).

3.5. Morphological Characterization of RΔFRGD NPs and the RΔFRGD-siNR4A1 Nanocomplex. The size and morphology of the RΔFRGD NPs and the RΔFRGD-siNR4A1 nanocomplex were studied using transmission electron microscopy and the experimental technique outlined previously.[30,31,38]

3.6. Stability of RΔFRGD NPs and the RΔFRGD-siNR4A1 Nanocomplex in the *In Vitro* Condition. To check the proteolytic stability, nonspecific and specific enzyme Proteinase K and trypsin were added to RΔFRGD NPs, followed by incubation for 6 h at room temperature with constant stirring at low rpm. Then, the treated samples were analyzed using Shimadzu RP-HPLC on a Phenomenex C-18 column as described in an earlier section. Enzyme-treated samples were also checked to observe the morphological change by TEM, and the imaging procedure has also been described earlier.[30,31,38] siNR4A1 stability in the nanocomplex was investigated by the addition of RNase A with the nanocomplex followed by incubating at room temperature for 6 h. The samples were run on a 3% agarose gel electrophoresis as described in an earlier section, and morphological changes were observed under TEM.[31,38]

3.7. Cell Culture. Cell lines (WRL 68, Hep G2, HEK 293T, Huh7) were maintained in a Dulbecco's modified Eagle's medium that was supplemented with 3.7 g of sodium bicarbonate and 3.7 g of HEPES. Additionally, the medium contained 10% fetal bovine serum (FBS) and 0.1% pen-strep. Each cell line was sustained in a humidified incubator at 37 °C with 5% CO_2 and was passed at a confluency of between 70 and 80%.

3.8. Cytotoxicity of RΔFRGD NPs and the RΔFRGD-siNR4A1 Nanocomplex in Different Mammalian Cell Lines. Cytotoxicities of lyophilized RΔFRGD NPs and the RΔFRGD-siNR4A1 nanocomplex were determined using the standard MTT assay for WRL 68, Hep G2, HEK 293T, and Huh7 cell lines. Cells were grown (5×10^3 cells/well) in 96-well sterile microtiter plates and allowed to grow for 18 h for proper cell adherence and treated with RΔFRGD NPs (39−773 μM) and the RΔFRGD-siNR4A1 nanocomplex MTT assay was performed as described earlier.[30]

3.9. *In Vitro* Hemolysis of RΔFRGD NPs and the RΔFRGD-siNR4A1 Nanocomplex. Human blood (10% citrate-phosphate−dextrose) was received from the Rotary Blood Bank (New Delhi, India). Red blood cells (RBCs) were harvested by centrifuging at 1500*g* for 10 min at 25 °C (3−5 washes with PBS). Further, 100 μL of the packed RBC suspension (10%, v/v) was transferred to a Corning 96-well microtiter plate and mixed with 100 μL of a peptide solution (39−773 μM) and the RΔFRGD-siNR4A1 nanocomplex (70−280 nM). The RBCs were incubated at 37 °C for 3 h and then centrifuged at 1500*g* for 10 min at 25 °C. The 100 μL supernatant was transferred to a new microtiter plate, and absorbance was measured at 540 nm using a microplate reader VersaMax ELISA reader to measure RBC lysis. Cells incubated with PBS and 0.2% Triton X-100 were used as controls. The degree of RBC destruction induced by the RΔFRGD NPs and the nanocomplex was recorded by estimating the amount of hemoglobin released after RBC damage.

3.10. *In Vitro* Inflammatory Response of RΔFRGD NPs. An enzyme-linked immunosorbent assay (ELISA) was used to quantify the amount of IFN-γ secreted by the T cells after incubating with RΔFRGD NPs in accordance with a previous report that we had published.[30]

3.11. Animal Experiments and Ethics. Animal experiments were performed according to the guidelines of the Institutional Animal Ethics Committee (IAEC), Centre for Comparative Medicine, Institute of Liver and Biliary Sciences (vide no. IAEC/ILBS/19/02).

3.12. Hepatic Stellate Cell Isolation and Characterization. Hepatic stellate cells (HSCs) were isolated from healthy SD rat liver through retrograde perfusion. Initially, the body weight of the animal was measured and intraperitoneal injections of ketamine (100 mg/kg/body weight) and xylazine (5 mg/kg/body weight) were given according to the body weight. The liver was exposed by making an incision in the upper abdomen. A 24-gauge catheter was inserted into the portal vein. Then, 200 mL of Hanks buffer solution was injected at a perfusion rate of 20 mL/min into the portal vein while leaving the inferior vena cava open as an outlet flow. Next, for *in vivo* enzymatic digestion, 150 mL of Hank's buffer containing 30 mg of collagenase type 1 was injected at the perfusion rate of 5 mL/min, and the IVC was ligated with the help of a thread. The perfused liver was then excised from the animal, minced, and transferred to 100 mL of Hanks buffer containing 10 mg of collagenase at 37 °C for *in vitro* digestion. Further, the digested liver tissue was passed through a 100 μm filter into 50 mL falcons containing Krebs, and these tubes were centrifuged at 50*g* for 5 min at 4 °C. The parenchymal population of the liver, i.e., the hepatocytes, settled down as a pellet, whereas the nonparenchymal population, i.e., the hepatic stellate cells, endothelial cells, and Kupffer cells, was present in the supernatant. Next, the supernatant was centrifuged at 800*g* for 10 min and resuspended in PBS. HSCs were extracted using a 50/25% percoll density gradient centrifugation at 800*g* for 25 min at 4 °C with 0 acceleration and deceleration. The topmost buffy layer containing HSCs was isolated and washed twice in PBS. The isolated HSCs were resuspended in IMDM media with 10% FBS and 1% antibiotic under standard culture conditions.

To characterize the isolated HSCs, the cells were fixed with 4% paraformaldehyde for 30 min at room temperature and washed thrice with PBS (5 min each). To permeabilize the fixed cells, they were then treated with 1% Triton X-100 for 20 min and washed twice with PBS. The cells were then incubated with primary antibodies (α-SMA) overnight at 4 °C. The excess antibody was removed, and the cells were washed twice with PBS and incubated with a secondary antibody for 2 h at room temperature. The cells were washed, and the images were acquired using an inverted fluorescence microscope (Leica systems).

3.13. *In Vitro* Cellular Uptake of Hepatic Stellate Cells. The fluorescent tagging procedure of RΔFRGD has been discussed in an earlier section. 1×10^4 HSC cells were seeded on a confocal dish (Corning 35 mm), and 24 h after seeding, the medium was replaced with 1 mL of complete medium. Then, the RΔFRGD (30 μg/mL) NPs and the

https://doi.org/10.1021/acsomega.2c05292
ACS Omega 2022, 7, 36811−36824

RΔFRGD-siNR4A1 nanocomplex containing 1 μg of fluorescein-labeled siNR4A1 were incubated with HSC cells. After 5 h of treatment, cells were carefully washed with incomplete media and PBS to remove the excess sample, and cellular uptake was visualized using a confocal laser microscope (Nikon A1r, Tokyo, Japan) in the FITC channel. The nucleus was stained with DAPI before imaging.

A flow cytometry experiment was also carried out to quantify the uptake of NPs and the nanocomplex by HSC cells. HSC cells were seeded at a cell density of 5×10^4 cells/well in a 12-well plate, and RΔFRGD NPs and the RΔFRGD-siNR4A1 nanocomplex were added in the same proportion as described earlier. The culture medium was removed after 5 h of incubation, followed by PBS washing and trypsinization. The cells were centrifuged at 2000 rpm for 10 min at 4 °C, and the resulting cell pellet was washed twice with ice-cold PBS. Cell suspensions were introduced into the FACS Aria III flow cytometer (BD Bioscience, San Jose, CA) within the next 30 min, and the data were analyzed using FlowJo v10 software. Cells without treatment were used as controls in flow cytometry studies.

3.14. Cirrhosis Induction by Carbon Tetrachloride (CCl_4). Healthy male Wistar rats weighing 175−200 g were injected with CCl_4 intraperitoneally thrice a week and received phenobarbital (0.3 g/L) in the drinking water. Animals developed micronodular cirrhosis after 8 weeks of CCl_4 injection, and CCl_4 administration was stopped after physical characterization of developed ascites, and treatment was provided after 1 week.

3.15. *In Vivo* Hepatic Tissue Biodistribution of RΔFRGD-FITC in Cirrhotic and Control Rats. For the *in vivo* hepatic tissue biodistribution experiment, RΔFRGD was first tagged with fluorescein isothiocyanate isomer I (FITC). FITC-tagged NPs were injected into control and cirrhotic rats ($n = 4$) intravenously at a single dose of 1.5 mg/kg. After 2 h postadministration, rats were euthanized. Liver from treated rats was excised, embedded in parafilm, and sectioned before imaging. For confocal microscopy, confocal laser scanning (Nikon A1r, Tokyo, Japan) under a Nikon microscope was used to observe the slide. The excitation wavelength for FITC was 488 nm (argon laser), and fluorescence was detected through an HQ 515/30 emission filter (high-quality band-pass). Images were processed using NIS Elements (Nikon) and Photoshop 6.0 (Adobe Systems, San Jose, CA) for the final image assembly.

3.16. *In Vivo* Silencing of NR4A1 Gene in an Experimental Liver Cirrhosis Rat Model. We next tested the effect of the RΔFRGD-siNR4A1 nanocomplex-mediated NR4A1 gene silencing in the liver of the cirrhotic rat model. Six weeks of CCl_4-treated rats were randomized into different groups for treatment, including RΔFRGD-siNR4A1 nanocomplex and RΔFRGD-Veh (scrambled siRNA) untreated healthy control and cirrhotic control. RΔFRGD-siNR4A1 nanocomplexes were injected intravenously at 0.1 mg/kg of body weight every 72 h twice/week for 2 weeks (four doses), along with continuous induction of CCl_4. The animals were sacrificed 1 week after the final injection, the liver was excised, their weight was recorded, and blood was collected.

3.17. Gene Expression Analysis Using Quantitative Real-Time PCR. Total RNA from the cells and tissues was isolated by the traditional trizol method. First, 0.5 mL of trizol reagent per 1×10^6 cells or 0.5 mg of tissue was used to lyse the cells. Chloroform was mixed and centrifuged for 10 min at 12,000*g* at 4 °C. The aqueous phase containing the RNA was separated into a fresh tube, incubated with prechilled isopropanol for 15 min, and later centrifuged for 10 min at 12,000*g* at 4 °C. Washing was performed with the resultant pellet containing the RNA with 0.5 mL of chilled 75% ethanol and centrifuged for 5 min at 7500*g* at 4 °C followed by DNase treatment. The RNA pellet was then air-dried for 5−10 min followed by the addition of 20 μL of nuclease-free water. To dissolve the pellet, incubation in a dry bath at 56 °C for 10−15 min was performed. Later, 1.5−2 μL of the isolated RNA was aliquoted for quantification with a nanodrop spectrophotometer, and the rest was stored at −80 °C.

The cDNA was prepared using a Thermo Scientific revert aid first strand cDNA synthesis kit (verso cDNA synthesis kit, Thermo Fisher Scientific). The following reagents were added in the indicated order: template RNA (0.1 ng−5 μg), random hexamer (1 μL), nuclease-free water (volume makeup), 5× reaction buffer (4 μL), ribolock RNase inhibitor (1 μL), 10 mM dNTP mix (2 μL), and revert aid M-MuLV RT (1 μL) (total volume 20 μL). After gently mixing the components, they were centrifuged and incubated for 5 min at 25 °C, followed by 60 min at 42 °C. The reaction was stopped after 5 min of heating at 70 °C.

Real-time PCR experiments were conducted using ViiA7 AB applied biosystems (Thermo Fisher Scientific). Reactions were performed in 20 μL volumes in 384-well plates containing 2 μL of forward primer, 2 μL of reverse primer, 4 μL of cDNA, 2 μL of nuclease-free water, and 10 μL of Sybr Green. The reaction conditions were as follows: 95 °C for 10 min (hold stage), then 40 cycles of 95 °C for 15 s, and 60 °C for 1 min (PCR stage), 95 °C for 15 s, and 60 °C for 1 min (melt curve stage). The relative gene expression was calculated for each sample using the $\Delta\Delta C_t$ method, and the expression values were normalized with housekeeping genes 18S. The primers used in the study are given in Table S1.

3.18. NR4A1 Protein-Level Determination Using Western Blotting. Livers from rats treated with the RΔFRGD-siNR4A1 nanocomplex and from control groups were excised and homogenized using a mortar and pestle with N_2. Total protein was extracted from homogenized livers of both groups using RIPA lysis buffer having a protease inhibitor cocktail (Thermo Fisher Scientific Inc., New York). The total protein concentration was estimated by the bicinchoninic acid (BCA) protein estimation kit (Thermo Scientific). Also, 60 μg of protein was separated by SDS-PAGE and transferred onto the nitrocellulose membrane (Millipore). The membrane was blocked with 5% skimmed milk in Tris-buffered saline (pH 7.3) for 2 h at room temperature. Then, blots were then incubated overnight at 4 °C with the primary NR4A1 monoclonal antibody (1:1000, Thermo Scientific), followed by three washes with TBS-T. The membrane was then incubated with the horseradish peroxidase-conjugated secondary antibody used at 1:10,000 (Sigma, St. Louis, MO) at room temperature for 2 h. Following three washes with PBS-T, the specific NR4A1 band was visualized using an ECL detection kit (Thermo Scientific). Similarly, GAPDH on the same membrane was probed as an internal control (Thermo Scientific). Densitometric analysis was performed with ImageJ, and relative quantitation of NR4A1 normalized to GAPDH was determined.

3.19. Hemodynamic Assessment and Biochemical Analysis. Animals were anesthetized by injecting ketamine hydrochloride (100 mg/kg; Neon Laboratories Ltd., Mumbai,

https://doi.org/10.1021/acsomega.2c05292
ACS Omega 2022, 7, 36811−36824

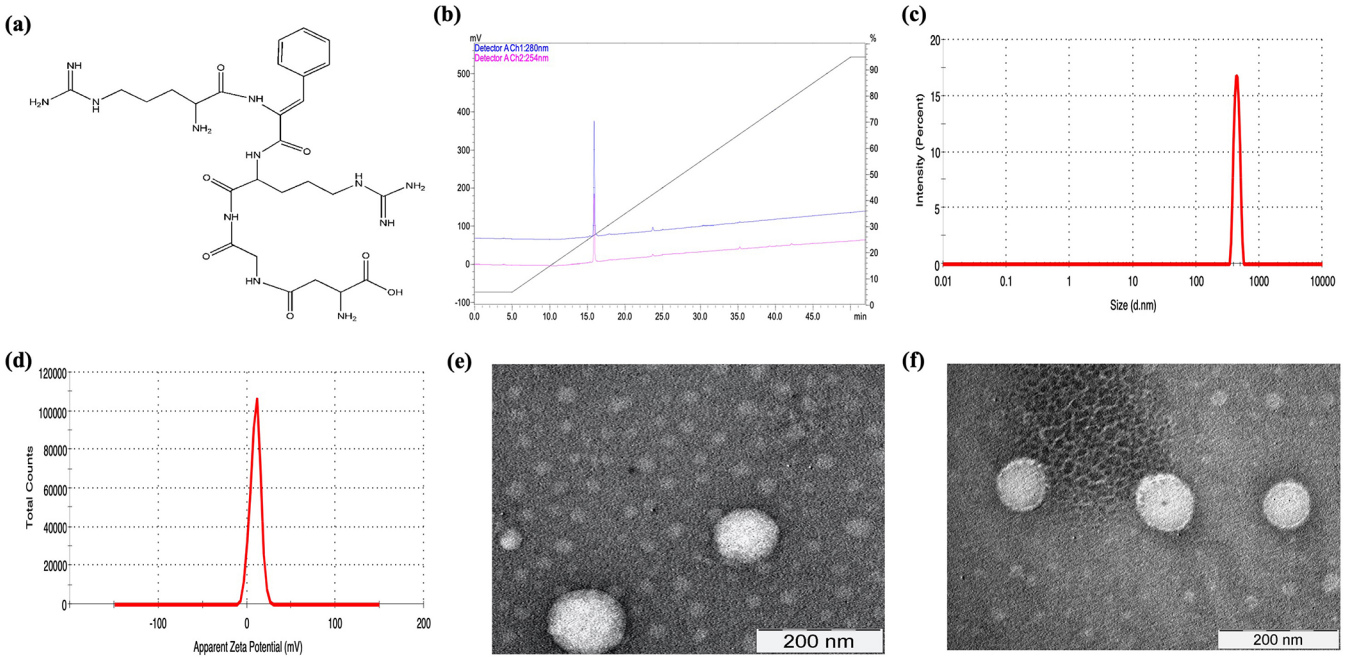

Figure 1. (a) Chemical structure of RΔFRGD. (b) RP-HPLC profile of RΔFRGD showing a single peak at RT-16 min. (c) Hydrodynamic diameter of RΔFRGD NPs at 2 mg/mL concentration. (d) ζ-Potential of RΔFRGD NPs studied using DLS. (e) Transmission electron microscopy image of RΔFRGD NPs. (f) Transmission electron micrograph for resuspended RΔFRGD NPs after lyophilization.

India) plus midazolam (5 mg/kg intraperitoneally; Neon Laboratories Ltd., Mumbai, India) intraperitoneally. The femoral artery and the ileocolic vein were cannulated with PE-50 fluid-filled catheters connected to a pressure transducer (Edwards Lifesciences, Irvine, CA) to measure the mean arterial pressure (MAP; mmHg) and portal pressure (PP; mmHg), respectively. Perivascular ultrasonic transit time flow probes connected to a flow meter (Transonic Systems, Ithaca, NY) were placed around the portal vein as close as possible to the liver to measure portal blood flow (PBF; mL/min/g) perfusing the liver and around the superior mesenteric artery in rats to measure superior mesenteric artery blood flow (SMABF, mL/min/100 g body weight). The flow probe and the two pressure transducers were connected to a PowerLab (4SP) linked to a computer using the Chart version 5.0.1 for Windows software (AD Instruments, Australia).

To measure the biochemical characteristics like serum liver enzymes, including aspartate aminotransferase and alanine aminotransferase, and bilirubin levels, a 1 mL venous blood sample was obtained at the end of each experiment. All biochemical measurements were conducted with standard methods at the Department of Biochemical Analysis, ILBS, Delhi.

3.20. Histopathology and Hepatic Fibrosis Analysis. Liver tissues excised from the animals were fixed in 10% formalin, embedded in paraffin, and cut into sections of a thickness of 2 μm; the sections were then mounted onto slides, and the slides were stained with hematoxylin and eosin. To evaluate the fibrosis, liver tissue sections were stained with Masson's Trichrome. The images were obtained with the EVOS-microscope at 10×, 20×, and 40×. The areas showing positive collagen deposition from the respective staining were quantified using Image J software. Eight to ten fields per sample were quantified and expressed as mean values.

3.21. Statistical Analysis. GraphPad Prism, version 6.01 (San Diego, CA), was used to perform the statistical analysis. The data has been presented as ± standard deviation. Differences were considered significant at a p-value <0.05.

4. RESULTS

4.1. Synthesis and Characterization of RΔFRGD. RΔFRGD was synthesized by solid-phase peptide synthesis methods and characterized by RP-HPLC and mass spectrometry. RΔFRGD and the corresponding saturated analogue eluted as a single peak with a retention time of 16 min (Figures 1b and S1b) and showed a molecular mass of 647.4 Da (Figure S1a).

4.2. Preparation and Characterization of RΔFRGD NPs. The pentapeptide-HFIP solution was mixed with water to initiate self-assembly of the peptide, and nanoparticle formation was assessed using DLS. DLS measurements showed that at a concentration of 2 mg/mL, RΔFRGD self-assembled into homogenous nanoparticles with a hydrodynamic diameter of 468.46 ± 11.95 nm, PDI 0.20 ± 0.011 (Figure 1c), and surface charge ~9.57 ± 0.50 mV (Figure 1d), and therefore, all other studies were carried out at this concentration. The TEM image indicated that the RΔFRGD NPs were spherical in shape with a diameter of 174.69 ± 10.42 nm (Figure 1e). The preformed NPs were lyophilized and resuspended in deionized water. The morphological characteristic, including the size and shape of the resuspended NPs, were reinvestigated using DLS and TEM analyses. The hydrodynamic diameter was observed after lyophilization, 377.53 nm (Figure S2a). No morphological changes in the nanoparticles post lyophilization were observed, with spherical nanoparticles of size (as observed by TEM) 164.56 ± 13.09 nm (Figure 1f).

4.3. Formation and Characterization of RΔFRGD-NR4A1 Nanocomplexes. To test whether the RΔFRGD NPs will form a stable nanocomplex with siNR4A1 (nuclear receptor subfamily 4, group A member), varying amounts of preformed RΔFRGD NPs were incubated with a fixed amount of siRNA (w/w). Condensation of siNR4A1 with RΔFRGD

https://doi.org/10.1021/acsomega.2c05292
ACS Omega 2022, 7, 36811−36824

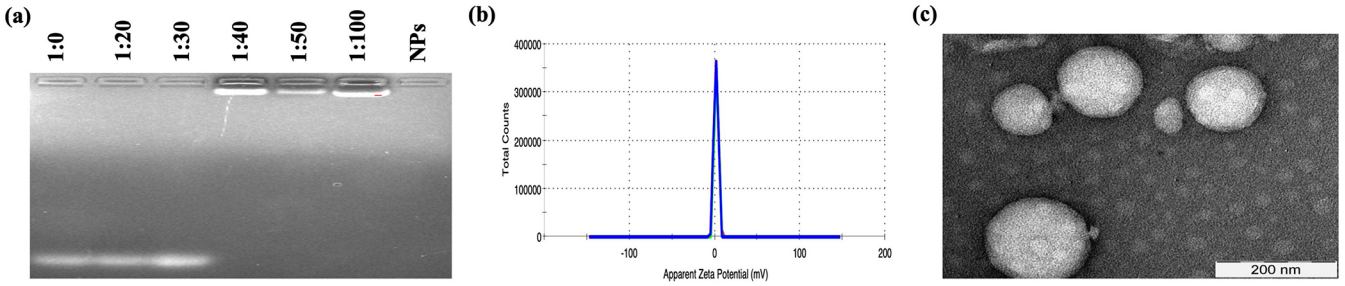

Figure 2. (a) Gel retardation assay showing complete complexation of siRN4A1 with RΔFRGD NPs at 1:40 (siNR4A1/RΔFRGD, w/w). (b) ζ-Potential of the RΔFRGD-siNR4A1 nanocomplex, 1.95 ± 0.18 mV (n = 3). (c) Transmission electron microscopy image of the RΔFRGD-siNR4A1 nanocomplex (n = 3).

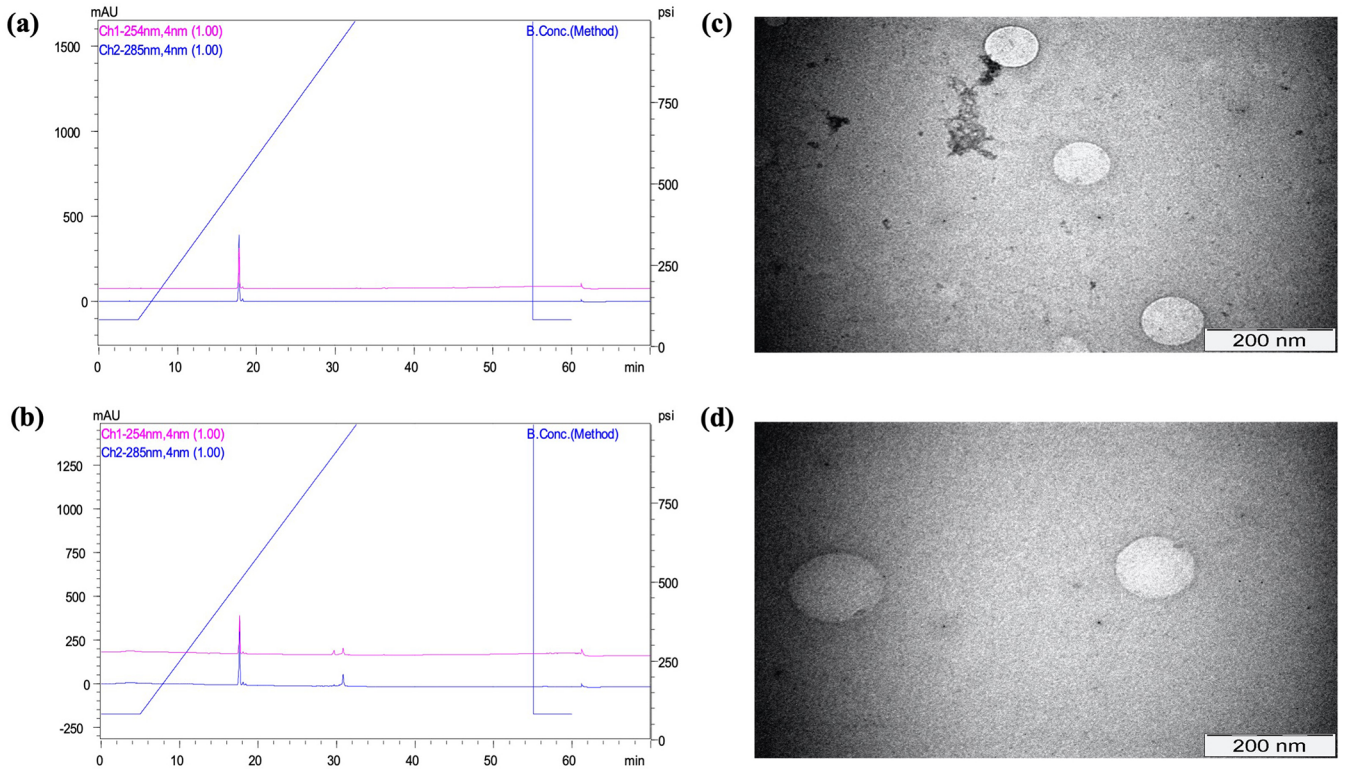

Figure 3. Proteolytic stability of RΔFRGD NPs after treatment with (a) proteinase K and (b) trypsin, analyzed using RP-HPLC. Morphological characterization of RΔFRGD NPs treated with (c) proteinase K and (d) trypsin, using TEM.

NPs was monitored by a gel retardation assay. The oligonucleotides being negatively charged moved toward the anode, but after the interaction of siNR4A1 with positively charged NPs, the mobility of the nanocomplex was restricted in the wells. Complete retardation of siNR4A1 was observed at a ratio of 1:40 (siNR4A1/RΔFRGD NPs) (Figure 2a). For further studies, the RΔFRGD-siNR4A1 nanocomplex was used at a ratio of 1:40 (siNR4A1/RΔFRGD NPs, w/w). After complexation with siNR4A1, the average ζ-potential of RΔFRGD NPs decreased to 1.95 ± 0.18 mV from ∼9.57 ± 0.50 mV (Figure 2b). TEM images of nanocomplexes showed a diameter of 185.89 ± 16.44 nm, and there were no significant changes in shape and size (Figure 2c).

4.4. Stability of RΔFRGD NPs and the RΔFRGD-siNR4A1 Nanocomplex in the *In Vitro* Condition. To test proteolytic stability under *in vitro* conditions, RΔFRGD NPs were treated with proteinase K and trypsin, and the degradation of the peptide was monitored using RP-HPLC and TEM for 6 h. The RP-HPLC profile showed that RΔFRGD NPs were completely able to protect from proteinase K until 6 h (Figures 3a and S2d), whereas the saturated analogue showed significant degradation (Figure S2c). However, in the case of trypsin, although there was observable degradation of RΔFRGD (Figures 3b and S2e), it was significantly more stable than the natural analogue, RFRGD, to trypsin treatment (Figure S2b). TEM images also showed no changes in morphological structures of RΔFRGD NPs after treatment with proteinase K (Figures 3c and S2f) and trypsin (Figures 3d and S2g). To check whether complexation of siNR4A1 with RΔFRGD can protect it from degradation by RNase, the RΔFRGD-siNR4A1 nanocomplex was treated with RNase A for 6 h. Agarose gel showed RΔFRGD NPs completely protected siNR4A1 from RNase A degradation (Figure S2h), and there were no observable morphological changes (Figure S2i).

4.5. *In Vitro* Biocompatibility of RΔFRGD NPs and the RΔFRGD-siNR4A1 Nanocomplex. To investigate whether the nanocomplex was cytotoxic, four different cell lines

https://doi.org/10.1021/acsomega.2c05292
ACS Omega 2022, 7, 36811−36824

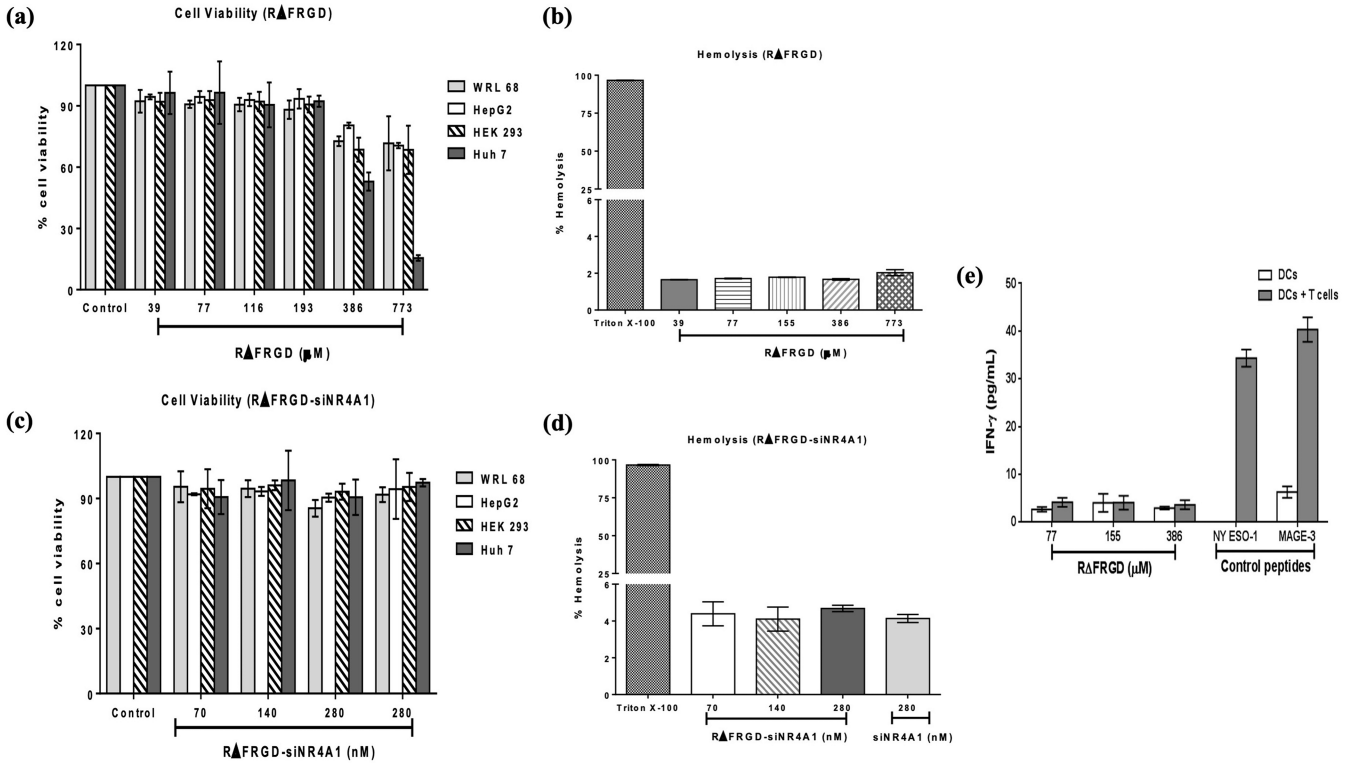

Figure 4. Cytotoxicity of RΔFRGD NPs and the RΔFRGD-siNR4A1 nanocomplex treated with four cell lines and monitored by the MTT assay. Percentage cell viability against WRL 68, Hep G2, Huh7, and HEK 293T cells treated with different concentrations of (a) RΔFRGD NPs and (c) RΔFRGD-siNR4A1 nanocomplex. (b, d) Percentage hemolysis for RΔFRGD NPs and the RΔFRGD-siNR4A1 nanocomplex. (e) IFN-γ response for RΔFRGD at different concentrations and two well-known peptide-based antigens as the positive control, NYESO-1 and MAGE-3, *in vitro* coculture of T cells with DCs. The data has been presented as mean ± standard deviation.

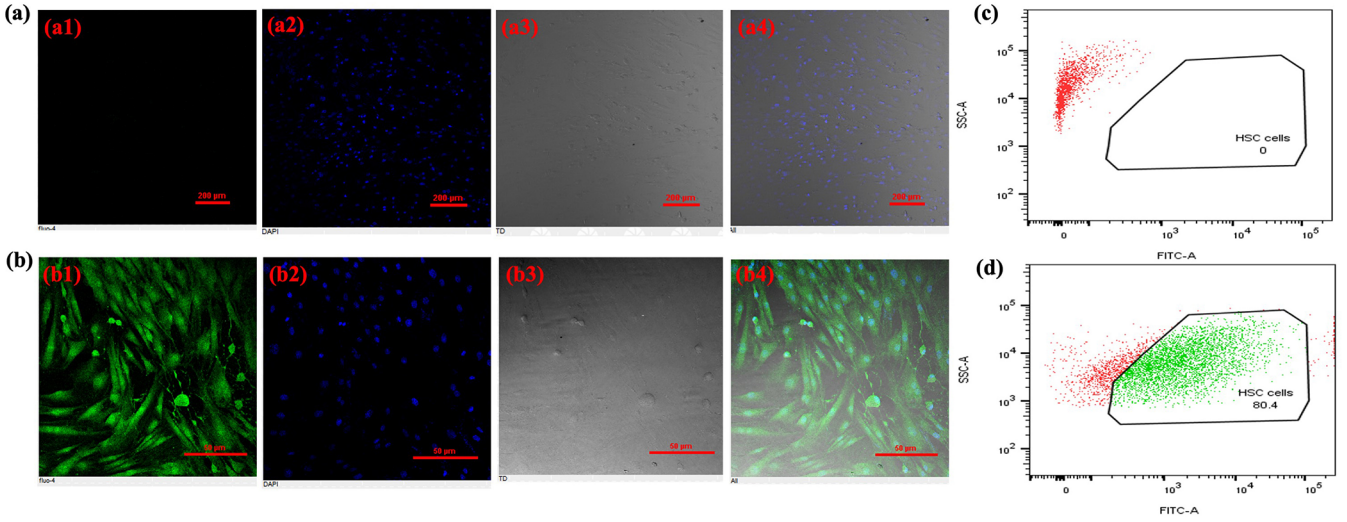

Figure 5. Confocal images showing the cellular uptake of nanoparticles in HSC cells, (a) untreated HSC cells, and (b) fluorescently labeled RΔFRGD NPs treated with HSC cells for 5 h (FITC channel in lane (a1, b1), nucleus labeled with DAPI in lane (a2, b2), a bright field in lane (a3, b3) and colocalization of all channels in lane (a4, b4)). Quantitative estimation of cellular uptake of HSCs by flow cytometry, (c) untreated cells (0.0%), and (d) HSCs treated with fluorescently labeled RΔFRGD NPs for 5 h and uptake observed was 80.4%.

including Huh7, Hep G2, HEK 293T, and WRL 68 were used and the cell viability followed by the standard MTT assay. No cellular toxicity (>90% viable cells) in any of the four cell lines was observed when treated with NPs up to a concentration of 193 μM (Figure 4a). The toxicity levels increased gradually at further concentrations after 193 μM for all cell lines. We observed that the siNR4A1 concentration up to 280 nM was not toxic to the four cell lines used (Figure 4c).

We also investigated if the RΔFRGD NPs and the RΔFRGD-siNR4A1 nanocomplex caused hemolysis for RBC, and to do this, the peptide was incubated with RBC, and the level of hemoglobin was measured by a spectrophotometer. The RΔFRGD NPs and the RΔFRGD-siNR4A1 nanocomplex

https://doi.org/10.1021/acsomega.2c05292
ACS Omega 2022, 7, 36811−36824

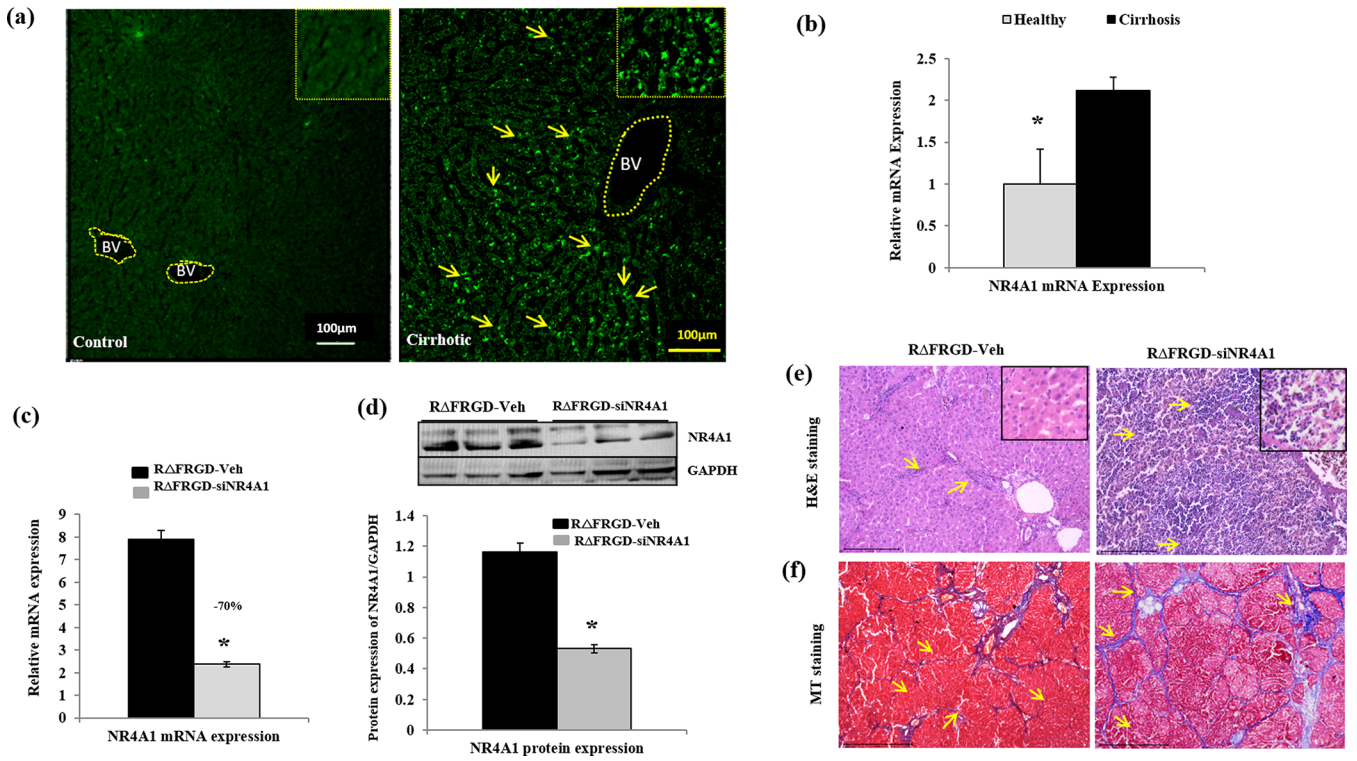

Figure 6. (a) Confocal microscopy images of healthy and cirrhotic rats intravenously administered with labeled RΔFRGD NPs, showing significant accumulation of the NPs in the liver of cirrhotic rats (n = 3). (b) NR4A1 mRNA expression in healthy and experimental liver cirrhotic rats (n = 6). (c) Quantitative real-time PCR (n = 6) and (d) relative protein expression of NR4A1 in cirrhotic liver treated with the RΔFRGD-siNR4A1 nanocomplex, determined by western blotting. Histopathological images for cirrhotic liver sections stained with (e) hematoxylin and eosin stain (H&E) indicating the presence of enhanced inflammatory cell infiltration in the group treated with the RΔFRGD-siNR4A1 nanocomplex (pericentral nuclei in blue) as compared to the vehicle group. (f) Masson's trichrome (MT) showing significant aggravation in hepatic fibrosis in the RΔFRGD-siNR4A1-treated group as the red stain has been pulled out by collagen in this group. *BV, blood vessels.

showed less than 5% hemolysis in a concentration ranging from 39 to 773 μM and 70 to 280 nM, respectively (Figure 4b,d). RΔFRGD NPs induced negligible IFN-γ response (less than 4 pg/mL) in a concentration range of 77−386 μM compared to NYESO-1 (34.33 pg/mL) and MAGE-3 (40.33 pg/mL) (Figure 4e).

4.6. *In Vitro* Cellular Uptake of RΔFRGD NPs and the RΔFRGD-siNR4A1 Nanocomplex by Primary Hepatic Stellate Cells. To investigate the uptake of RΔFRGD NPs *in vitro*, we isolated and characterized primary hepatic stellate cells from rat liver, using collagenase enzymatic digestion, followed by density gradient centrifugation. For characterization of primary HSC cells, cultured cells were fixed and immunolabeled with α-SMA, and bright-green fluorescence was observed for αSMA positive cells (Figure S3a).

Next, to investigate whether RΔFRGD NPs and RΔFRGD-siNR4A1 nanocomplexes were readily taken by HSC cells, fluorescently labeled RΔFRGD NPs and RΔFRGD-siNR4A1 nanocomplexes were incubated with HSCs for 5 h followed by confocal laser microscopy and flow cytometry. The presence of bright-green fluorescence distributed inside the cells indicated efficient cellular uptake of RΔFRGD NPs and the RΔFRGD-siNR4A1 nanocomplex (Figures 5b and S3b). Cellular uptakes of ∼80.4 and ∼87.7% were observed for cells treated with RΔFRGD and the RΔFRGD-siNR4A1 nanocomplex (Figures 5d and S3c) with respect to untreated cells, respectively.

4.7. *In Vivo* Hepatic Tissue Biodistribution of RΔFRGD-FITC in Cirrhotic and Control Rats. To evaluate the specificity of the new targeted RΔFRGD NPs toward the liver cirrhotic region, RΔFRGD was first labeled with FITC and evaluated under a laser-scanning fluorescence microscope. FITC conjugated NPs (1.5 mg/kg body weight) were predominantly accumulated in the cirrhotic liver as compared to the control liver, and the fluorescence of tagged RΔFRGD NPs was specifically found in the perisinusoidal and perivascular regions of the liver (Figure 6a); the mean fluorescence was significantly higher in the case of the cirrhotic liver (587.84 ± 2.49) as compared to the normal liver (Figure S4d). Importantly, no adverse event was noticed. Also, no significant biochemical and physiological changes were observed.

4.8. *In Vivo* Silencing of the NR4A1 Gene in Cirrhotic Liver, mRNA and Protein Expression Analysis. *In vivo* expression of NR4A1 in experimental and control liver tissues was analyzed by quantitative gene expression in all of the experimental groups. In comparison to the healthy controls, NR4A1 was overexpressed in cirrhotic conditions (Figure 6b). mRNA expression of NR4A1 was significantly downregulated (−70%) in RΔFRGD-siNR4A1 nanocomplex-treated groups in comparison to RΔFRGD-Veh treated animals. Hence, a significant NR4A1 gene knockdown was achieved after treatment with the RΔFRGD-siNR4A1 nanocomplex in the experimental cirrhotic model (Figure 6c).

In liver tissues, the protein expression of NR4A1 was analyzed, and it was observed that the RΔFRGD-siNR4A1 nanocomplex-treated group showed significantly lower levels of the NR4A1/GAPDH ratio (−55%) and translational effect of NR4A1 gene inhibition *in vivo* (Figures 6d and S4a−c).

https://doi.org/10.1021/acsomega.2c05292
ACS Omega 2022, 7, 36811−36824

Table 1. Effects of RΔFRGD-veh/siNR4A1 on Hepatic and Systemic Hemodynamic in CCl_4 Experimental Cirrhotic Rats[a]

	CCl_4 cirrhotics			
parameters	healthy	RΔFRGD-Veh	RΔFRGD-siNR4A1	*p*-value
MAP (mmHg)	129 ± 16	100 ± 15*	97 ± 8*	$p < 0.05$*
PP (mmHg)	6.7 ± 1.2	11.8 ± 1.5*	14.0 ± 1.3*#	$p < 0.05$*#
PBF (mL/min)	9.8 ± 3.2	14.37 ± 4.4*	16.2 ± 5.1*	$p < 0.05$*#
HVR (mmHg/mL·min·g^{-1})	6.6 ± 2.0	10.8 ± 1.68*	13.9 ± 2.4*#	$p < 0.05$*#
HR (beats/min)	364 ± 38	313 ± 23	302 ± 43*	NS

[a]CCl_4, carbon tetrachloride; MAP, mean arterial pressure; PP, portal pressure; PBF, portal blood flow; HVR, hepatic vascular resistance; HR, heart rate. Values represent mean ± standard deviation. *$p < 0.05$ vs controls; #$p < 0.05$ vs siVeh.

Table 2. Effects of RΔFRGD-veh/siNR4A1 on Biochemical Parameters in CCl_4 Experimental Cirrhotic Rats[a]

	CCl_4 cirrhotics			
characteristics	healthy	RΔFRGD-Veh	RΔFRGD-siNR4A1	*p*-value
AST (U/L)	83 ± 16	193 ± 15*	177 ± 25*	$p < 0.05$*
ALT (U/L)	43 ± 11	134.5 ± 18*	109.7 ± 23*	$p < 0.05$*
total bilirubin (mg/dL)	0.4 ± 0.1	0.9 ± 0.4*	0.7 ± 0.6*	$p < 0.05$*
liver weight	7.3 ± 1.8	13.08 ± 2*	14.7 ± 2.5*	$p < 0.05$*
spleen mass	0.7 ± 0.12	0.83 ± 0.18	0.91 ± 0.13	NS
body weight	369 ± 46	359 ± 50	404 ± 70	NS

[a]CCl_4, carbon tetrachloride; AST, aspartate aminotransferase; ALT, alanine aminotransferase. Values represent mean ± standard deviation. *$p < 0.05$ vs controls; #$p < 0.05$ vs siVeh.

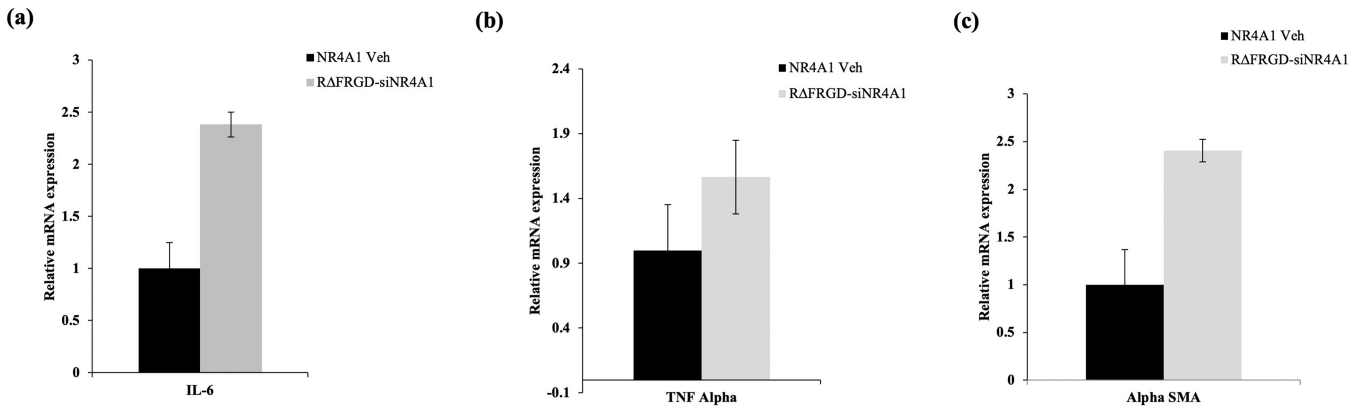

Figure 7. Relative mRNA expression analysis of inflammatory markers for (a) IL-6, (b) TNF-α, and (c) α-SMA for RΔFRGD-Veh and RΔFRGD-siNR4A1 nanocomplexes.

4.9. Effect of NR4A1 Inhibition on Hepatic and Systemic Hemodynamic in Experimental Liver Cirrhosis. *In vivo* NR4A1 inhibition exaggerates the portal pressure in experimental liver cirrhosis. In comparison to healthy animals, we observed an obvious increase in portal pressure (PP) (+76%, $p < 0.02$), hepatic vascular resistance (HVR) (+63%, $p < 0.04$), and portal blood flow (PBF) (+45%, $p < 0.05$) in the experimental cirrhotic RΔFRGD-Veh group. We also noticed significant systemic hypotension assessed by a reduction in the mean arterial pressure (−20%, $p < 0.05$) in the RΔFRGD-Veh group. Further, the finding reveals that early *in vivo* inhibition of NR4A1 in experimental cirrhosis aggravated the PP (+18%, $p < 0.05$). The increment in PP was supplemented by raised HVR (+28%, $p < 0.05$) and PBF (+13%, $p = 0.12$) in the RΔFRGD-siNR4A1 nanocomplex in comparison to the RΔFRGD-Veh group. The systemic and hepatic hemodynamic parameters are shown in Table 1.

4.10. Effects of NR4A1 Inhibition on Liver Function in CCl_4-Cirrhotic Rats. We observed a significant elevation in the level of liver enzymes in the RΔFRGD-Veh- and RΔFRGD-siNR4A1-treated cirrhotic groups in comparison to healthy controls. There were no significant differences in the level of liver enzymes and bilirubin between RΔFRGD-Veh- and RΔFRGD-siNR4A1-treated cirrhotic groups. We did not observe any significant changes in hepatic, splenic mass, and total body weight of experimental cirrhotic animals. However, the liver weight was significantly high in cirrhotic animals in comparison to healthy controls, while spleen and body weight was marginally high, but the difference was not statistically significant (Table 2).

4.11. Effect of Liver-Specific NR4A1 Knockdown on Experimental Cirrhosis and Inflammation. CCl_4 cirrhotic rats showed evidence of expected deformation of the hepatic parenchyma due to excess deposition of collagen in the space of disse and establishment of fibrotic septa within liver parenchyma as evaluated by Masson's trichrome staining (Figure 6f).

As shown in Figure 6f, *in vivo* early inhibition of NR4A1 produced a significant aggravation in hepatic fibrosis in RΔFRGD-siNR4A1 (+41% in MT stain)-treated rats in

https://doi.org/10.1021/acsomega.2c05292
ACS Omega 2022, 7, 36811−36824

comparison to RΔFRGD-Veh groups. Similarly, periseptal, perivascular, and periportal inflammatory cell infiltration was quite evident in the RΔFRGD-siNR4A1 nanocomplex-treated group compared to the vehicle-treated rats in H&E staining (Figure 6e). Moreover, αSMA, a surrogate marker of HSC activation and fibrosis, was significantly high (>2-fold, $p < 0.05$) in the RΔFRGD-siNR4A1 nanocomplex group in comparison to RΔFRGD-Veh groups. In addition, proinflammatory markers interleukins (IL-6; >2-fold, $p < 0.05$) and tumor necrosis factor α (TNFα; >1.5-fold, NS), were markedly raised in the RΔFRGD-siNR4A1 nanocomplex group in comparison to RΔFRGD-Veh rats (Figure 7a−c). Importantly, aggravation in hepatic fibrosis and inflammation confirmed the loss of function of the NR4A1 gene and protein in liver tissues.

5. DISCUSSION

Liver fibrosis and cirrhosis remain major public health concerns throughout the world.[7] Although clinical evidence suggests that liver fibrosis can be reversed, there are no standard antifibrotic molecules for clinical use due to limited efficacy and adverse effects.[39] Gene therapy could be a potential alternative, but the lack of an efficient gene delivery system to the fibrotic liver has been a major obstacle in harnessing its therapeutic potential.[40] Targeted delivery platforms may have the potential to precisely deliver oligonucleotides at the required site.[15]

In the past few decades, the use of positively charged nano vehicle systems has become an active area of research in nonviral vector gene delivery systems. Cationic NPs can readily condense negatively charged oligonucleotides and also facilitate their entry through the cell membrane and avoid premature degradation.[41,42] Different modified cationic lipids including, diamine-type cholesteryl-3-carboxamide, cyclic 3,4-dihydroxy-pyrrolidinium, DOTMA/Chol, and polymers including PVA-chitosan and mPEG-PLGA-PLL, and succinylated PEI-based NPs have been explored for oligonucleotide delivery, but their complex synthesis and comparatively low biocompatibility and nondegradability have hampered their acceptance of use in biomedical application.[43−48] In recent years, many cationic peptide-based nano vehicle systems for DNA/RNA delivery have been explored, but their high susceptibility toward proteolytic degradation has restricted their clinical development.[49] Researchers have utilized different strategies including peptide cyclization, conjugation of bulky groups, the inclusion of nonprotein amino acids, etc., to resolve stability issues.[50] Dipeptides containing noncoded α,β-dehydro amino acid, namely, α,β-dehydrophenylalanine, at their C-terminal have shown tremendous potential to form different self-assembled nanostructures with high proteolytic stability.[24−28] Out of a panel of modified dipeptides, RΔF forms highly stable nanospheres of size 60−80 nm, which was found to condense plasmid DNA, protected it from enzymatic degradation, and delivered efficiently.[31] Therefore, the incorporation of RΔF in a sequence not only helps in peptide self-assembly into NPs but also provides them with high proteolytic stability.

Liver cirrhosis is a condition characterized by enormous fibrosis due to excess deposition of extracellular matrix and activation of HSCs. In normal liver, HSCs are in a quiescent state, while on injury, they get transformed into myofibroblasts, which can proliferate and produce inflammatory responses, leading to a massive accumulation of extracellular cellular matrix.[19] As HSCs play a key role in liver fibrosis, many researchers have explored HSCs as therapeutic targets for liver fibrosis. Many ligands targeting HSCs have been explored for delivery purposes, but most of them are unable to differentiate between aHSCs and qHSCs. The tripeptide RGD was found to have a high binding affinity toward integrin αvβ3 and collagen VI receptors overexpressed on activated aHSCs while bypassing qHSCs.[19,51,52] Therefore, linear RGD and its cyclic versions have been widely investigated for targeting liver fibrosis.[51] Here, we have designed a pentapeptide containing RΔF, as a self-assembling template, and RGD, as a targeting ligand.

The pentapeptide, RΔFRGD, was synthesized using standard Fmoc chemistry, purified, and characterized by RP-HPLC and mass spectroscopy. Self-assembly of the pentapeptide was initiated by dissolving it into a mixture of HFIP and water. As evidenced by DLS and TEM imaging, the peptide readily self-assembled into uniform spherical nanoparticles of ∼174 nm size. In general, spherical NPs of size 10−200 nm have been shown to provide a longer half-life and enhanced cellular permeability under *in vivo* conditions.[53] The pentapeptide NPs were carefully lyophilized and resuspended in sterile water before use. There was no change in the size or morphology of the NPs upon lyophilization and resuspension.

Small RNA molecules like siRNAs have been shown to affect a wide variety of cellular processes, including cell proliferation, migration, and apoptosis through different pathways.[54] In this study, we have attempted to deliver a well-known siRNA related to liver fibrosis, i.e., siNR4A1, using pentapeptide-based NPs as a proof of principle.[34−36] Also, it is pertinent to point out here that the expression of NR4A1 negatively correlates with liver fibrosis. First, we investigated whether RΔFRGD NPs will form a stable complex with siNR4A1. The complexation of siNR4A1 with RΔFRGD NPs at different siRNA/peptide ratios was tracked using a gel retardation assay. Our results showed that at a ratio of 1:40 (siRNA/RΔFRGD NPs), complete retardation of siNR4A1 occurred, indicating the formation of a stable nanocomplex. Here, the electrostatic interaction between the overall positive charge on the pentapeptide and the negative charge on the siRNA seems to play a crucial role in the process of complexation. Kostarelos et al. have also shown the complexation of siRNA with positively charged peptide-based nanofibers (PNFs).[55] The complexation process was also followed using ζ-potential measurements, and we observed a significant decrease in the ζ-potential of RΔFRGD NPs after complexation with siNR4A1. Thus, nanocomplexation seems to be an outcome of the electrostatic interaction between siRNA and the peptide NPs. These results were comparable to and even better than the results of earlier studies. For example, Zhao et al. have reported the formation of chitosan-coated PLGA NPs with a ζ-potential of +6.35 mV, and the loading of a plasmid DNA with NPs was carried out at a ratio of 0.5:100 (DNA/NPs).[46] Further, Duan et al. have reported the formation of mPEG-PLGA-PLL-based NPs with a ζ-potential of +11.4 mV, and siRNA was loaded at a ratio of 1:600 (siRNA/NPs).[47] Voshavar et al. have shown the formation of PLGA-lipid NPs with a ζ-potential of +30.05 mV, and siRNA condensation was carried out at a ratio of ∼1:300 (siRNA/NPs).[43] Also, neutral or low charge particles are reported to have minimum interaction with serum proteins and are more suitable for receptor binding and nanoparticle internalization.[56,57] Next, to investigate morphological changes in the peptide NPs upon complexation, TEM imaging was carried out. Our results showed that there were no observable

https://doi.org/10.1021/acsomega.2c05292
ACS Omega 2022, 7, 36811−36824

changes in the size, shape, and morphology of the NPs after complexation with the siRNA.

An ideal oligonucleotide delivery system should have a longer half-life and provide protection to oligonucleotides from endonucleases under *in vivo* conditions.[28] To investigate the proteolytic stability of RΔFRGD, the NPs were treated with two proteases, proteinase K (a nonspecific protease) and trypsin (a serine protease), and the stability was monitored using RP-HPLC. Our results showed that RΔFRGD was relatively more stable than RFRGD (a saturated analogue) to proteolytic degradation. Next, we checked whether the peptide NPs would be able to protect siRNA from degradation by RNase. For this, the nanocomplex was exposed to RNase A, and the degradation was followed on the agarose gel. Our results showed that RΔFRGD NPs protected siNR4A1 completely when present in the condensed form from the degradation by RNase A.

The biocompatibility of nano delivery systems plays a key role in their clinical development.[58,59] *In vitro* cellular toxicity for RΔFRGD NPs and RΔFRGD-siNR4A1 was determined using Huh7, Hep G2, WRL 68, and HEK 293T cell lines. Cells treated with the peptide NPs and the nanocomplex showed >90% cell viability, which indicated high biocompatibility not only for the delivery vehicle but also for the nanocomplex. These results clearly indicated the suitability of the nano delivery system for use in *in vivo* applications. Lysis of RBCs caused by different nanoparticle formulations is another key factor to be considered for their *in vivo* use.[60] Both peptide RΔFRGD NPs and the nanocomplex showed less than 5% hemolysis, which is under the limits prescribed by the ISO/TR 7406 guidelines for biomaterials.[61] Further, it is also desirable that the nanocarrier system should not induce any inflammatory response.[62] Our results showed that RΔFRGD NPs did not elicit inflammatory cytokine response, IFN-γ. The nonimmunotoxic and highly biocompatible nature of RΔFRGD NPs makes them suitable candidates for use in different biomedical applications. It is crucial for a vehicle system to not only reach the target site but also enter cells and deliver its cargo inside the cells. Therefore, cellular uptake of RΔFRGD NPs and the RΔFRGD-siNR4A1 nanocomplex was studied in HSCs. The results of confocal microscopy and flow cytometry studies showed that both the peptide NPs and the nanocomplex were readily taken up by HSCs.

One of the major attributes of a successful delivery system is to deliver its functional cargos to the required site by circumventing enroute barriers under *in vivo* conditions. It is well known that all nano delivery systems injected intravenously reach the liver, but due to the high intrahepatic flow rate, they are washed out rapidly.[63] To test whether RGD containing pentapeptide NPs will accumulate at the liver cirrhotic site, the fluorescently labeled NPs were checked for hepatic biodistribution in normal and cirrhotic rats. Our results showed that there was a significant accumulation of RΔFRGD NPs in the liver of cirrhotic rats compared to normal rats. Also, within the liver of cirrhotic rats, the peptide NPs were specifically accumulated in perisinusoidal and peri-vascular regions. Additionally, no adverse event or significant biochemical and physiological changes were observed in rats injected with the RΔFRGD NPs, thereby indicating their high *in vivo* biocompatibility.

Next, we investigated whether the nanocomplex can be delivered to the cirrhotic liver and followed the efficacy of delivered siRNA by measuring gene and protein expression levels upon intravenous injection. Animals treated with the RΔFRGD-siNR4A1 nanocomplex showed significant downregulation of the NR4A1 gene (−70%), which clearly indicated that the pentapeptide-based vehicle system not only protected siNR4A1 from endonucleases but also successfully delivered it to the cirrhotic site. Since silencing of the NR4A1 gene results in downregulation of the NR4A1 protein, the functionality of siRNA delivered was also confirmed by protein expression studies using Western blot analysis. Our results showed a considerable reduction in the NR4A1 protein expression compared to the untreated group (55%). It has been well reported that the deficiency in the NR4A1 gene aggravates skin, lung, and liver fibrosis, which results in enhanced inflammation at the fibrotic liver site.[34,64−67] To further confirm the silencing of the NR4A1 gene by siNR4A1 under *in vivo* conditions, the inflammatory markers were monitored using real-time PCR and histopathology analyses. Results of real-time PCR showed significantly increased levels of IL-6, TNF-α, and α-SMA markers compared to the untreated group. Similarly, histopathology images of the RΔFRGD-siNR4A1 nanocomplex-treated group showed considerably enhanced inflammation with massive immune cell infiltration as compared to the untreated group. As expected, silencing of the NR4A1 gene aggravated fibrosis and altered hepatic vascular resistance, which resulted in an increase in portal pressure in the nanocomplex-treated group. As mentioned earlier that this is a proof-of-principle study to see if we can specifically deliver any siRNA to the liver cirrhosis site, these results could be of use for researchers working on developing NR4A1-specific therapeutic targets. Ease of synthesis, characterization, target specificity, high stability, and, most importantly, high biocompatibility of these pentapeptide-based NPs make them suitable for further development for therapeutic purposes.

6. CONCLUSIONS

In this study, we have designed, synthesized, and characterized a novel pentapeptide containing a self-assembling dipeptide template and a specific tripeptide ligand for homing to the fibrotic liver site. Results from our *in vitro* and *in vivo* studies have demonstrated that the pentapeptide-based NPs are highly stable, readily complexed with well-known siRNA, protected it from the action of endonuclease, and delivered to the liver cirrhotic site. This study highlights the potential of the pentapeptide-based system as an efficient delivery platform for siRNA/small molecules and adds new dimensions to emerging nonviral-based gene delivery and its application in therapeutic purposes.

■ ASSOCIATED CONTENT

Supporting Information

The Supporting Information is available free of charge at https://pubs.acs.org/doi/10.1021/acsomega.2c05292.

Syntheses of RΔF azlactone, RΔFRGD, and RΔFRGD-FITC; mass spectrometry of RΔFRGD; RP-HPLC of RFRGD; hydrodynamic diameter of resuspended RΔFRGD NPs; proteolytic stability of NPs (RP-HPLC and TEM); stability of the nanocomplex toward RNase A action (agarose gel electrophoresis and TEM); HSC characterization by fluorescence microscopy; cellular uptake of HSCs using confocal microscopy and

https://doi.org/10.1021/acsomega.2c05292
ACS Omega 2022, 7, 36811−36824

flow cytometry; and uncropped western blot protein expressions of NR4A1 and GAPDH (PDF)

AUTHOR INFORMATION

Corresponding Authors

Dinesh M. Tripathi − *Institute of Liver and Biliary Sciences, New Delhi, Delhi 110070, India*; Phone: +91-11-46300000; Email: dineshmanitripathi@gmail.com

Virander Singh Chauhan − *International Centre for Genetic Engineering and Biotechnology, New Delhi, Delhi 110067, India*; orcid.org/0000-0001-9875-9549; Phone: +91-11-26741358; Email: viranderschauhan@gmail.com

Authors

Saikat Biswas − *International Centre for Genetic Engineering and Biotechnology, New Delhi, Delhi 110067, India*; orcid.org/0000-0002-9667-678X

Nitin Yadav − *International Centre for Genetic Engineering and Biotechnology, New Delhi, Delhi 110067, India*

Pinky Juneja − *Institute of Liver and Biliary Sciences, New Delhi, Delhi 110070, India*

Akash Kumar Mourya − *Institute of Liver and Biliary Sciences, New Delhi, Delhi 110070, India*

Savneet Kaur − *Institute of Liver and Biliary Sciences, New Delhi, Delhi 110070, India*

Complete contact information is available at: https://pubs.acs.org/10.1021/acsomega.2c05292

Notes

The authors declare no competing financial interest.

ACKNOWLEDGMENTS

This work was supported by the Department of Biotechnology, Government of India (BT/PR2573/NNT/28/534/2011) and the Science & Engineering Research Board (SERB), Government of India (SRG/2019/002128). The authors also acknowledge the Department of Science and Technology, Government of India (SB/S2/JCB-41/2014), the Department of Biotechnology, Government of India (BT/HRD/35/07/VSC/2015), and the Biotechnology Industry Research Assistance Council, Government of India (BIRAC/CCAMP0770/BIG-13/18) for financial support. The authors are really thankful to Dr. Prafulla Kumar Tailor for his support and suggestion during the cytokine experiment; Dr. Syed Shams Yazdani for providing RNase A; Dr. Paushali Mukherjee for her help during the data analysis; Tenzin Choedon, Girish HR, and Purnima kumari for their assistance in transmission electron microscopy, mass spectrometry, and confocal microscopy, respectively; Saurabh Yadav for his help in experiments to address the reviewer's comments; and Elluri Seetharami Reddy for his assistance and guidance during the data analysis of flow cytometric studies. The authors declare no conflicting interests. This manuscript was written entirely by the author with no outside assistance.

REFERENCES

(1) GBD 2017 Disease and Injury Incidence and Prevalence Collaborators. Global, regional, and national incidence, prevalence, and years lived with disability for 354 diseases and injuries for 195 countries and territories, 1990-2017: a systematic analysis for the Global Burden of Disease Study. *Lancet* **2017**, *392*, 1789−1858.

(2) Subramaniyan, V.; Chakravarthi, S.; Jegasothy, R.; Seng, W. Y.; Fuloria, N. K.; Fuloria, S.; Hazarika, I.; Das, A. Alcohol-associated liver disease: A review on its pathophysiology, diagnosis and drug therapy. *Toxicol. Rep.* **2021**, *8*, 376−385.

(3) Katarey, D.; Verma, S. Drug-induced liver injury. *Clin. Med.* **2016**, *16*, s104−s109.

(4) Schon, H. T.; Bartneck, M.; Borkham-Kamphorst, E.; Nattermann, J.; Lammers, T.; Tacke, F.; Weiskirchen, R. Pharmacological Intervention in Hepatic Stellate Cell Activation and Hepatic Fibrosis. *Front. Pharmacol.* **2016**, *7*, 33.

(5) Geerts, A. History, heterogeneity, developmental biology, and functions of quiescent hepatic stellate cells. *Semin. Liver Dis.* **2001**, *21*, 311−335.

(6) Kisseleva, T. The origin of fibrogenic myofibroblasts in fibrotic liver. *Hepatology* **2017**, *65*, 1039−1043.

(7) Schuppan, D.; Afdhal, N. H. Liver cirrhosis. *Lancet* **2008**, *371*, 838−851.

(8) Chang, Y.; Li, H. Hepatic Antifibrotic Pharmacotherapy: Are We Approaching Success? *J. Clin. Transl. Hepatol.* **2020**, *8*, 222−229.

(9) Xing, L.; Chang, X.; Shen, L.; Zhang, C.; Fan, Y.; Cho, C.; Zhang, Z.; Jiang, H. Progress in drug delivery system for fibrosis therapy. *Asian J. Pharm. Sci.* **2021**, *16*, 47−61.

(10) Popov, Y.; Schuppan, D. Targeting liver fibrosis: strategies for development and validation of antifibrotic therapies. *Hepatology* **2009**, *50*, 1294−1306.

(11) Bulaklak, K.; Gersbach, C. A. The once and future gene therapy. *Nat. Commun.* **2020**, *11*, No. 5820.

(12) Mali, S. Delivery systems for gene therapy. *Indian J. Hum. Genet.* **2013**, *19*, 3−8.

(13) Tatiparti, K.; Sau, S.; Kashaw, S. K.; Iyer, A. K. siRNA Delivery Strategies: A Comprehensive Review of Recent Developments. *Nanomaterials* **2017**, *7*, 77.

(14) Yu, B.; Zhao, X.; Lee, L. J.; Lee, R. J. Targeted delivery systems for oligonucleotide therapeutics. *AAPS J.* **2009**, *11*, 195−203.

(15) Poilil Surendran, S.; George Thomas, R.; Moon, M. J.; Jeong, Y. Y. Nanoparticles for the treatment of liver fibrosis. *Int. J. Nanomed.* **2017**, *12*, 6997−7006.

(16) Beljaars, L.; Molema, G.; Schuppan, D.; Geerts, A.; De Bleser, P. J.; Weert, B.; Meijer, D. K.; Poelstra, K. Successful targeting to rat hepatic stellate cells using albumin modified with cyclic peptides that recognize the collagen type VI receptor. *J. Biol. Chem.* **2000**, *275*, 12743−12751.

(17) Beljaars, L.; Molema, G.; Weert, B.; Bonnema, H.; Olinga, P.; Groothuis, G. M.; Meijer, D. K.; Poelstra, K. Albumin modified with mannose 6-phosphate: A potential carrier for selective delivery of antifibrotic drugs to rat and human hepatic stellate cells. *Hepatology* **1999**, *29*, 1486−1493.

(18) Blume, G.; Cevc, G.; Crommelin, M. D.; Bakker-Woudenberg, I. A.; Kluft, C.; Storm, G. Specific targeting with poly(ethylene glycol)-modified liposomes: coupling of homing devices to the ends of the polymeric chains combines effective target binding with long circulation times. *Biochim. Biophys. Acta, Biomembr.* **1993**, *1149*, 180−184.

(19) Li, Y.; Pu, S.; Liu, Q.; Li, R.; Zhang, J.; Wu, T.; Chen, L.; Li, H.; Yang, X.; Zou, M.; Xiao, J.; Xie, W.; He, J. An integrin-based nanoparticle that targets activated hepatic stellate cells and alleviates liver fibrosis. *J. Controlled Release* **2019**, *303*, 77−90.

(20) Lehto, T.; Ezzat, K.; Wood, M.; El Andaloussi, S. Peptides for nucleic acid delivery. *Adv. Drug Delivery Rev.* **2016**, *106*, 172−182.

(21) Habibi, N.; Kamaly, N.; Memic, A.; Shafiee, H. Self-assembled peptide-based nanostructures: Smart nanomaterials toward targeted drug delivery. *Nano Today* **2016**, *11*, 41−60.

(22) Panda, J. J.; Chauhan, V. S. Short peptide-based self-assembled nanostructures: implications in drug delivery and tissue engineering. *Polym. Chem.* **2014**, *5*, 4431−4449.

(23) Bruno, B. J.; Miller, G. D.; Lim, C. S. Basics and recent advances in peptide and protein drug delivery. *Ther. Delivery* **2013**, *4*, 1443−1467.

(24) Gupta, M.; Bagaria, A.; Mishra, A.; Mathur, P.; Basu, A.; Ramakumar, S.; Chauhan, V. S. Self-Assembly of a Dipeptide-

Containing Conformationally Restricted Dehydrophenylalanine Residue to Form Ordered Nanotubes. *Adv. Mater.* **2007**, *19*, 858−861.
(25) Mishra, A.; Panda, J. J.; Basu, A.; Chauhan, V. S. Nanovesicles based on self-assembly of conformationally constrained aromatic residue containing amphiphilic dipeptides. *Langmuir* **2008**, *24*, 4571−4576.
(26) Alam, S.; Panda, J. J.; Chauhan, V. S. Novel dipeptide nanoparticles for effective curcumin delivery. *Int. J. Nanomed.* **2012**, *7*, 4207−4222.
(27) Panda, J. J.; Kaul, A.; Alam, S.; Babbar, A. K.; Mishra, A. K.; Chauhan, V. S. Designed peptides as model self-assembling nanosystems: characterization and potential biomedical applications. *Ther. Delivery* **2011**, *2*, 193−204.
(28) Panda, J. J.; Kaul, A.; Kumar, S.; Alam, S.; Mishra, A. K.; Kundu, G. C.; Chauhan, V. S. Modified dipeptide-based nanoparticles: vehicles for targeted tumor drug delivery. *Nanomedicine* **2013**, *8*, 1927−1942.
(29) Anand, G.; Biswas, S.; Yadav, N.; Mukherjee, P.; Chauhan, V. S. Production and Immunogenicity of a Tag-Free Recombinant Chimera Based on PfMSP-1 and PfMSP-3 Using Alhydrogel and Dipeptide-Based Hydrogels. *Vaccines* **2021**, *9*, 782.
(30) Verma, P.; Biswas, S.; Yadav, N.; Khatri, A.; Siddiqui, H.; Panda, J. J.; Rawat, B. S.; Tailor, P.; Chauhan, V. S. Delivery of a Cancer-Testis Antigen-Derived Peptide Using Conformationally Restricted Dipeptide-Based Self-Assembled Nanotubes. *Mol. Pharmaceutics* **2021**, *18*, 3832−3842.
(31) Panda, J. J.; Varshney, A.; Chauhan, V. S. Self-assembled nanoparticles based on modified cationic dipeptides and DNA: novel systems for gene delivery. *J. Nanobiotechnol.* **2013**, *11*, 18.
(32) Yamada, K. M. Fibronectin peptides in cell migration and wound repair. *J. Clin. Invest.* **2000**, *105*, 1507−1509.
(33) Ezhilararasan, D.; Lakshmi, T.; Raut, B. Novel Nano-Based Drug Delivery Systems Targeting Hepatic Stellate Cells in the Fibrotic Liver. *J. Nanomater.* **2021**, *2021*, 1−9.
(34) Palumbo-Zerr, K.; Zerr, P.; Distler, A.; Fliehr, J.; Mancuso, R.; Huang, J.; Mielenz, D.; Tomcik, M.; Fürnrohr, B. G.; Scholtysek, C.; Dees, C.; Beyer, C.; Krönke, G.; Metzger, D.; Distler, O.; Schett, G.; Distler, J. H. Orphan nuclear receptor NR4A1 regulates transforming growth factor-β signaling and fibrosis. *Nat. Med.* **2015**, *21*, 150−158.
(35) Zeng, X.; Yue, Z.; Gao, Y.; Jiang, G.; Zeng, F.; Shao, Y.; Huang, J.; Yin, M.; Li, Y. NR4A1 is Involved in Fibrogenesis in Ovarian Endometriosis. *Cell. Physiol. Biochem.* **2018**, *46*, 1078−1090.
(36) Feng, G.; Zhang, Z.; Dang, M.; Zhang, X.; Doleyres, Y.; Song, Y.; Chen, D.; Ma, P. X. Injectable nanofibrous spongy microspheres for NR4A1 plasmid DNA transfection to reverse fibrotic degeneration and support disc regeneration. *Biomaterials* **2017**, *131*, 86−97.
(37) Panda, J. J.; Dua, R.; Mishra, A.; Mittra, B.; Chauhan, V. S. 3D cell growth and proliferation on a RGD functionalized nanofibrillar hydrogel based on a conformationally restricted residue containing dipeptide. *ACS Appl. Mater. Interfaces* **2010**, *2*, 2839−2848.
(38) Thota, C. K.; Yadav, N.; Chauhan, V. S. A novel highly stable and injectable hydrogel based on a conformationally restricted ultrashort peptide. *Sci. Rep.* **2016**, *6*, No. 31167.
(39) Chen, Z.; Jain, A.; Liu, H.; Zhao, Z.; Cheng, K. Targeted Drug Delivery to Hepatic Stellate Cells for the Treatment of Liver Fibrosis. *J. Pharmacol. Exp. Ther.* **2019**, *370*, 695−702.
(40) Kamimura, K.; Suda, T.; Zhang, G.; Liu, D. Advances in Gene Delivery Systems. *Pharm. Med.* **2011**, *25*, 293−306.
(41) Peer, D.; Karp, J. M.; Hong, S.; Farokhzad, O. C.; Margalit, R.; Langer, R. Nanocarriers as an emerging platform for cancer therapy. *Nat. Nanotechnol.* **2007**, *2*, 751−760.
(42) Strebhardt, K.; Ullrich, A. Paul Ehrlich's magic bullet concept: 100 years of progress. *Nat. Rev. Cancer* **2008**, *8*, 473−480.
(43) Desai, P. R.; Marepally, S.; Patel, A. R.; Voshavar, C.; Chaudhuri, A.; Singh, M. Topical delivery of anti-TNFα siRNA and capsaicin via novel lipid-polymer hybrid nanoparticles efficiently inhibits skin inflammation in vivo. *J. Controlled Release* **2013**, *170*, 51−63.
(44) Hattori, Y.; Hara, E.; Shingu, Y.; Minamiguchi, D.; Nakamura, A.; Arai, S.; Ohno, H.; Kawano, K.; Fujii, N.; Yonemochi, E. siRNA delivery into tumor cells by cationic cholesterol derivative-based nanoparticles and liposomes. *Biol. Pharm. Bull.* **2015**, *38*, 30−38.
(45) Wang, X.; Yu, B.; Ren, W.; Mo, X.; Zhou, C.; He, H.; Jia, H.; Wang, L.; Jacob, S. T.; Lee, R. J.; Ghoshal, K.; Lee, L. J. Enhanced hepatic delivery of siRNA and microRNA using oleic acid based lipid nanoparticle formulations. *J. Controlled Release* **2013**, *172*, 690−698.
(46) Zhao, K.; Zhang, Y.; Zhang, X.; Shi, C.; Wang, X.; Wang, X.; Jin, Z.; Cui, S. Chitosan-coated poly(lactic-co-glycolic) acid nanoparticles as an efficient delivery system for Newcastle disease virus DNA vaccine. *Int. J. Nanomed.* **2014**, *9*, 4609−4619.
(47) Du, J.; Sun, Y.; Shi, Q. S.; Liu, P. F.; Zhu, M. J.; Wang, C. H.; Du, L. F.; Duan, Y. R. Biodegradable nanoparticles of mPEG-PLGA-PLL triblock copolymers as novel non-viral vectors for improving siRNA delivery and gene silencing. *Int. J. Mol. Sci.* **2012**, *13*, 516−533.
(48) Zintchenko, A.; Philipp, A.; Dehshahri, A.; Wagner, E. Simple modifications of branched PEI lead to highly efficient siRNA carriers with low toxicity. *Bioconjugate Chem.* **2008**, *19*, 1448−1455.
(49) Panda, J. J.; Chauhan, V. S. Short peptide based self-assembled nanostructures: implications in drug delivery and tissue engineering. *Polym. Chem.* **2014**, *5*, 4431−4449.
(50) Yadav, N.; Chauhan, M. K.; Chauhan, V. S. Short to ultrashort peptide-based hydrogels as a platform for biomedical applications. *Biomater. Sci.* **2020**, *8*, 84−100.
(51) Ruoslahti, E. RGD and other recognition sequences for integrins. *Annu. Rev. Cell Dev. Biol.* **1996**, *12*, 697−715.
(52) Li, D.; Friedman, S. L. Liver fibrogenesis and the role of hepatic stellate cells: new insights and prospects for therapy. *J. Gastroenterol. Hepatol.* **1999**, *14*, 618−633.
(53) Hoshyar, N.; Gray, S.; Han, H.; Bao, G. The effect of nanoparticle size on in vivo pharmacokinetics and cellular interaction. *Nanomedicine* **2016**, *11*, 673−692.
(54) Zhang, C. Novel functions for small RNA molecules. *Curr. Res. Mol. Ther.* **2009**, *11*, 641−651.
(55) Mazza, M.; Hadjidemetriou, M.; de Lázaro, I.; Bussy, C.; Kostarelos, K. Peptide nanofiber complexes with siRNA for deep brain gene silencing by stereotactic neurosurgery. *ACS Nano* **2015**, *9*, 1137−1149.
(56) Murugan, K.; Choonara, Y. E.; Kumar, P.; Bijukumar, D.; du Toit, L. C.; Pillay, V. Parameters and characteristics governing cellular internalization and trans-barrier trafficking of nanostructures. *Int. J. Nanomed.* **2015**, *10*, 2191−2206.
(57) Salatin, S.; Maleki Dizaj, S.; Yari Khosroushahi, A. Effect of the surface modification, size, and shape on cellular uptake of nanoparticles. *Cell Biol. Int.* **2015**, *39*, 881−890.
(58) Naahidi, S.; Jafari, M.; Edalat, F.; Raymond, K.; Khademhosseini, A.; Chen, P. Biocompatibility of engineered nanoparticles for drug delivery. *J. Controlled Release* **2013**, *166*, 182−194.
(59) Li, X.; Wang, L.; Fan, Y.; Feng, Q.; Cui, F. Biocompatibility and Toxicity of Nanoparticles and Nanotubes. *J. Nanomater.* **2012**, *2012*, No. 548389.
(60) Pan, D. C.; Myerson, J. W.; Brenner, J. S.; Patel, P. N.; Anselmo, A. C.; Mitragotri, S.; Muzykantov, V. Nanoparticle Properties Modulate Their Attachment and Effect on Carrier Red Blood Cells. *Sci. Rep.* **2018**, *8*, No. 1615.
(61) Guo, S.; Shi, Y.; Liang, Y.; Liu, L.; Sun, K.; Li, Y. Relationship and improvement strategies between drug nanocarrier characteristics and hemocompatibility: What can we learn from the literature. *Asian J. Pharm. Sci.* **2021**, *16*, 551−576.
(62) Rudra, J. S.; Sun, T.; Bird, K. C.; Daniels, M. D.; Gasiorowski, J. Z.; Chong, A. S.; Collier, J. H. Modulating adaptive immune responses to peptide self-assemblies. *ACS Nano* **2012**, *6*, 1557−1564.
(63) Tsoi, K. M.; MacParland, S. A.; Ma, X. Z.; et al. Mechanism of hard-nanomaterial clearance by the liver. *Nat. Mater.* **2016**, *15*, 1212−1221.
(64) Hamers, A. A. J.; Argmann, C.; Moerland, P. D.; Koenis, D. S.; Marinković, G.; Sokolović, M.; de Vos, A. F.; de Vries, C. J.; van Tiel,

https://doi.org/10.1021/acsomega.2c05292
ACS Omega 2022, 7, 36811−36824

C. M. Nur77-deficiency in bone marrow-derived macrophages modulates inflammatory responses, extracellular matrix homeostasis, phagocytosis and tolerance. *BMC Genomics* **2016**, *17*, 162.
(65) Pei, L.; Castrillo, A.; Chen, M.; Hoffmann, A.; Tontonoz, P. Induction of NR4A orphan nuclear receptor expression in macrophages in response to inflammatory stimuli. *J. Biol. Chem.* **2005**, *280*, 29256−29262.
(66) Hanna, R. N.; Shaked, I.; Hubbeling, H. G.; Punt, J. A.; Wu, R.; Herrley, E.; Zaugg, C.; Pei, H.; Geissmann, F.; Ley, K.; Hedrick, C. C. NR4A1 (Nur77) deletion polarizes macrophages toward an inflammatory phenotype and increases atherosclerosis. *Circ. Res.* **2012**, *110*, 416−427.
(67) Kurakula, K.; Vos, M.; Logiantara, A.; Roelofs, J. J.; Nieuwenhuis, M. A.; Koppelman, G. H.; Postma, D. S.; van Rijt, L. S.; de Vries, C. J. Nuclear Receptor Nur77 Attenuates Airway Inflammation in Mice by Suppressing NF-κB Activity in Lung Epithelial Cells. *J. Immunol.* **2015**, *195*, 1388−1398.

https://doi.org/10.1021/acsomega.2c05292
ACS Omega 2022, 7, 36811−36824